# Dynamics of resonant and nonresonant electron tunneling in double-quantum-well structures under electric fields

Toshio Matsusue
*Institute of Industrial Science, University of Tokyo, 7-22-1 Roppongi, Minato-ku, Tokyo 106, Japan*

Masahiro Tsuchiya
*Institute of Industrial Science, University of Tokyo, 7-22-1 Roppongi, Minato-ku, Tokyo 106, Japan and Sakaki Quantum Wave Project, Research Development Corporation of Japan, 4-3-24 Komaba, Meguro-ku, Tokyo 153, Japan*

J. N. Schulman*
*Research Center for Advanced Science and Technology, University of Tokyo, 4-6-1 Komaba, Meguro-ku, Tokyo 153, Japan*

Hiroyuki Sakaki
*Institute of Industrial Science, University of Tokyo, 7-22-1 Roppongi, Minato-ku, Tokyo 106, Japan; Research Center for Advanced Science and Technology, University of Tokyo, 4-6-1 Komaba, Meguro-ku, Tokyo 153, Japan; and Sakaki Quantum Wave Project, Research Development Corporation of Japan, 4-3-24 Komaba, Meguro-ku, Tokyo 153, Japan*

(Received 6 March 1990)

Tunneling processes of two-dimensional electrons between two quantum wells (QW's) and those from one QW to unconfined three-dimensional states outside through another QW are investigated in various double-QW structures by time-resolved photoluminescence (PL) measurements. Electric fields $F_z$ across the double-QW structures are applied to realize on- and off-resonance conditions, and the electron lifetime and time-integrated PL intensity are measured as functions of the field $F_z$. The experiment has demonstrated the enhancement of the tunneling rate near the resonance and its reduction under the off-resonance condition. The measured tunneling rates are compared with various theoretical models to show that a scattering-assisted process plays a dominant role in interwell tunneling when the ground levels of the two QW's are nearly resonant. At a certain bias voltage above resonance, a distinct reduction of the electron lifetime is observed and is attributed to LO-phonon-assisted tunneling into the other QW.

## I. INTRODUCTION

Tunneling and interference of electron waves are among the most important quantum-mechanical phenomena in ultrathin semiconductor heterostructures. Combined phenomena of tunneling and interference are particularly important for both physics and applications since they influence in a variety of ways electrical and optical characteristics, as already demonstrated in such structures as double-barrier resonant tunneling (DBRT) diodes[1,2] and superlattices.[3] So far, mainly static features of the tunneling phenomena have been investigated,[4] while dynamic aspects, in spite of their importance, have not been studied thoroughly.[5–24] This is mainly because the characteristic time scale of the process is of the order of picoseconds or less, which is shorter than that measurable by commonly available methods. Furthermore, theoretical studies have not been well developed, mainly because of the lack of reliable theoretical approaches to take proper account of scattering. Nevertheless, the dynamics should be investigated since it not only determines the ultimate speed of tunneling devices, but it elucidates fundamental aspects of electronic waves in solids, particularly their behaviors in time domain.

In order to discuss the resonant tunneling, the following two representative processes should be distinguished. In one process, unconfined three-dimensional (3D) electrons tunnel to a confined two-dimensional (2D) state in a quantum well (QW) or vice versa.[5–10] This process, which we denote as a 2D-3D process hereafter, is relevant to the dynamics of electrons in DBRT diodes. In another process, 2D electrons tunnel between two coupled QW's.[11–24] This 2D-2D process is relevant to electron transport in multi-QW structures under electric fields. In this process, tunneling can be affected by various interference effects between an initial QW state and a final QW state. Consequently, the dynamics is expected to be complicated and quite different from the 2D-3D process.

In order to clarify the dynamics of electron tunneling, we have adopted time-resolved photoluminescence (PL) spectroscopy. In a previous study, we first investigated the 2D-3D resonant tunneling in double-barrier structures, where we determined the intrinsic tunnel escape time,[6] and successfully explained the data using a theory that included nonparabolicity in the dispersion relation of

 

electrons via a two-band $\mathbf{k}\cdot\mathbf{p}$ theory.[25] This work has led us to understand fundamental aspects of the 2D-3D resonant tunneling.

In this work, we have extended our optical study of tunneling to investigate the 2D-2D tunneling process between two coupled QW's. The tunneling process of 2D electrons in one QW through another QW to unconfined 3D states was also studied. We clarify roles of the relation processes both in resonant tunneling and in off-resonant tunneling by comparing observed tunneling rates with various models. While a part of our work has been reported,[12,15,16,22,24] Oberli *et al.* have independently studied electron tunneling processes between two coupled QW's by a similar optical method.[18,23] They have examined, in particular, those cases where the ground level of one well is near the second level of the other well and where the two ground levels are apart. They have investigated the intersubband scattering time which determines the tunneling time between QW's and also the enhancement of tunneling rate which may be ascribed to LO-phonon scattering.[23] In the present paper we plan to provide complementary insights by investigating the tunneling process in somewhat different structures, where the two "ground" states are scanned systematically by electric fields to cover various resonant conditions. We have also analyzed both PL decay time and time-integrated PL intensity of both QW's. In addition, this work includes tunneling into unconfined 3D states through a QW.

We study mainly two kinds of double-quantum-well structures which have the potential profiles shown in Fig. 1. The "left" quantum well (LQW) with a well width of 71 Å is coupled with the "right" quantum well (RQW) with a well width of 51 Å through a thin central barrier with a thickness of 31 Å. The left barrier is made sufficiently thick (100 Å), whereas the right barrier has a thickness of 31 Å for sample I and 100 Å for sample II. All the barriers consist of pure AlAs, while both QW's are made of GaAs. Under the flat band condition of Fig. 1(a), the calculated ground level of LQW and RQW are 69.0 and 112.5 meV, above the bottom of the conduction band, respectively. We investigate the tunneling dynamics of electrons in these structures under electric fields.

The tunneling dynamics of electrons is expected to vary with electric field as schematically shown in Fig. 1 for sample I. Under the flat-band condition [Fig. 1(a)] and also the "below-resonance" condition, where the ground level $E_{L1}$ of electrons in LQW is below that $E_{R1}$ of RQW, the tunneling probability of electrons from the left well to the right electrode through RQW will be small, since the wave function of $E_{L1}$ in the right well has very small amplitude. Under the resonance condition [Fig. 1(b)], the ground levels of both QW's coincide and electrons tunnel back and forth between the two wells (tunnel oscillation). The mathematics of the level coupling and the tunnel oscillation process is described in Appendixes A and B. As a result, the tunnel escape rate of electrons from LQW to the right electrode will be enhanced. When the electric field is made further negative [Fig. 1(c)], the ground level of LQW goes above that of RQW. In such an "above-resonance" condition, the penetration of the wave function to RQW decreases again. Hence, the escape rate from LQW by "direct" tunneling to the outside decreases. In this case, some electrons may tunnel into RQW and scatter into the ground level $E_{R1}$ of RQW and finally escape to the outside by tunneling (scattering-assisted tunneling escape process).

In order to clarify which tunneling processes are dominant in actual systems, we have examined, under different electric fields, tunneling times and densities of electrons in each QW by measuring the PL decay time $\tau$ and the time-integrated PL intensity $I$ of each QW. Note that it is important to measure both $\tau$ and $I$ to analyze the tunneling mechanism.

In the following, we describe the experimental procedures in Sec. II. In Sec. III, we present the experimental data of PL decay time and time-integrated PL intensity to show how they change with applied electric fields. We then discuss the tunneling mechanisms by comparing

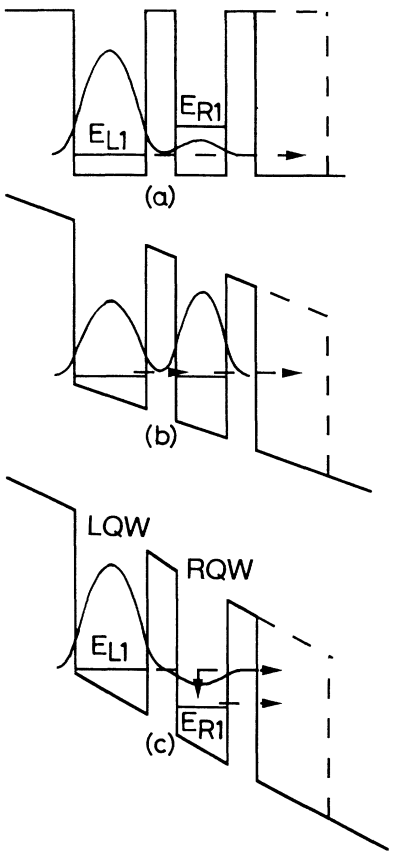


FIG. 1. Schematic illustrations of wave functions and tunneling processes of electrons associated mainly with the left quantum well in a coupled-quantum-well structure (solid line, sample I) under three representative conditions. Dashed line represents a thicker right barrier for sample II. Figures (a), (b), and (c) correspond, respectively, to "below"-resonance, on resonance, and "above"-resonance conditions, where the energy level associated with the left quantum well is lower than, equal to, and higher than that of the right quantum well.

the data with theoretical models. We first examine the electron dynamics for the case where the ground levels of the two QW's deviate slightly from the resonant condition. There we show that the tunnel escape through a QW is dominated by the scattering-assisted tunneling mechanism (accompanied by energy relaxation processes). We also discuss how the energy broadening of the quantum levels affect the strength and the sharpness of the resonance condition in actual structures. Next, we analyze the electron dynamics under off-resonant conditions, where the two ground levels are well separated; there we clarify the suppression of the tunnel escape process and investigate the contribution of the inelastic scattering, especially that of the LO-phonon-assisted tunneling.

## II. EXPERIMENTAL PROCEDURES

We prepared by molecular-beam epitaxy three double-quantum-well structures (samples I, II, and III). The structures of samples I and II were described earlier. Sample III is identical with sample II except that the central barrier is made thicker (57 Å). Sample III is studied to investigate how the tunneling process reduces as the central barrier becomes thicker. The samples were grown on (001) surfaces of semi-insulating GaAs substrates at 600 °C. First, we grew a superlattice buffer layer [5 periods of (500 Å GaAs)/(50 Å $Al_{0.3}Ga_{0.7}As$)], a 0.7-$\mu$m-thick $n$-type Si-doped GaAs layer ($N_d \sim 8\times10^{17}$ $cm^{-3}$), 500 Å undoped GaAs, and then one of the three undoped double-QW structures (samples I, II, and III). After growing a double-QW structure, 200 Å $Al_{0.3}Ga_{0.7}As$, and 200 Å GaAs were grown as a cap layer. The layer thicknesses were strictly controlled by monitoring the intensity oscillation of reflection high-energy electron diffraction (RHEED). Also, to get smooth heterointerfaces, the molecular-beam epitaxial (MBE) growth was interrupted at each interface for 1 min.[26] All epitaxial layers are of high quality with an estimated residual acceptor (carbon) concentration of $10^{14}-10^{15}$ $cm^{-3}$. On the sample surfaces, semitransparent Au Schottky contacts were formed in order to apply electric fields to the tunneling structures.

As shown schematically in Fig. 2, the tunneling processes in these samples were investigated at 20 K by monitoring time variation of PL intensity after generation of electrons (and holes) in both QW's with mode-locked dye laser pulses. The photoluminescence from each QW (Fig. 3) was selected by a monochromator, and detected by a synchro-scan streak camera (Hamamatsu C1587) for time-resolved measurements. Time-integrated PL intensity was also measured by a photomultiplier tube. The pulse width of the laser was less than 10 ps and the full width at half maximum (FWHM) of the time resolution of our detection system was typically $\sim$70 ps.

Electron-hole pairs were generated in both QW's in approximately equal amounts in order to monitor the electron concentrations both in RQW and LQW. To generate the same number of electrons and holes in both QW's over the whole range of applied voltage, the photon energy of the laser pulse was adjusted to be above the energy of $e$1-lh1 and below the energy of $e$2-hh2 for both QW's. Here, $ei$-hh$j$ ($ei$-lh$j$) indicates the transition between the $i$th subband of electrons and the $j$th subband of heavy (light) holes. The high-energy electrons and holes created in the QW's are expected to relax to quasi-thermal-equilibrium states inside each QW with very fast ($<$ several picoseconds) processes including intrasubband energy relaxation and also the transition from the lh1 to the hh1 states. The concentration of these photogenerated electrons decreases either by recombination (radiative and nonradiative) processes or by tunneling processes; this decrease is reflected in the decay time of the PL intensity. Hence, one can monitor the time variation of the electron concentrations, which is strongly affected by tunneling. Since the mass of the heavy hole is quite large in our samples, hole tunneling can be neglected at least in the initial phase of the tunneling process. Instead, those holes are accumulated mainly in the QW's with some steady-state concentration. These holes have a negligible influence on the electron tunneling process, as will be described later. If we deal with a quantum well where the light-hole state and heavy-hole state are mixed, then the hole tunneling has to be carefully taken into account.

## III. EXPERIMENTAL DATA AND THEORETICAL ANALYSIS

We first present in Fig. 3 the time-integrated PL and photoluminescence excitation (PLE) spectra of sample I measured at 20 K under several bias conditions: (1) flat band, (2) the beginning of the quasiresonance region, (3) the resonance, (4) the end of the quasiresonance region, (5) the above-resonance condition. These bias conditions will be discussed in detail later with reference to Fig. 5.

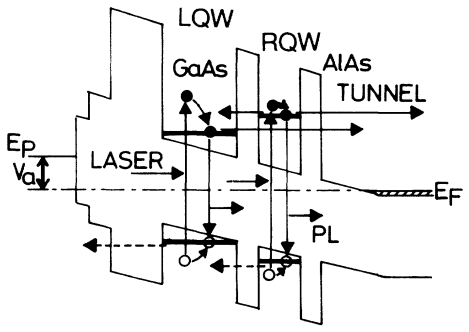


FIG. 2. Schematic illustration of our coupled-quantum-well (CQW) system and various dynamic processes of photogenerated carriers for the below-resonance condition. $E_F$ denotes the Fermi level of the $n^+$-type GaAs region underlying the CQW structure and $E_P$ indicates the Fermi (or pinning) level at the surface, where a Schottky contact is formed. $V_a$ is applied voltage. Solid and open circles indicate photogenerated electrons and holes, respectively; their dynamical processes are indicated by arrows that represent such processes as excitation by a laser pulse, relaxation inside each QW, tunneling, and radiative recombination resulting in photoluminescence (PL). Bold lines denote the energy levels of QW's.

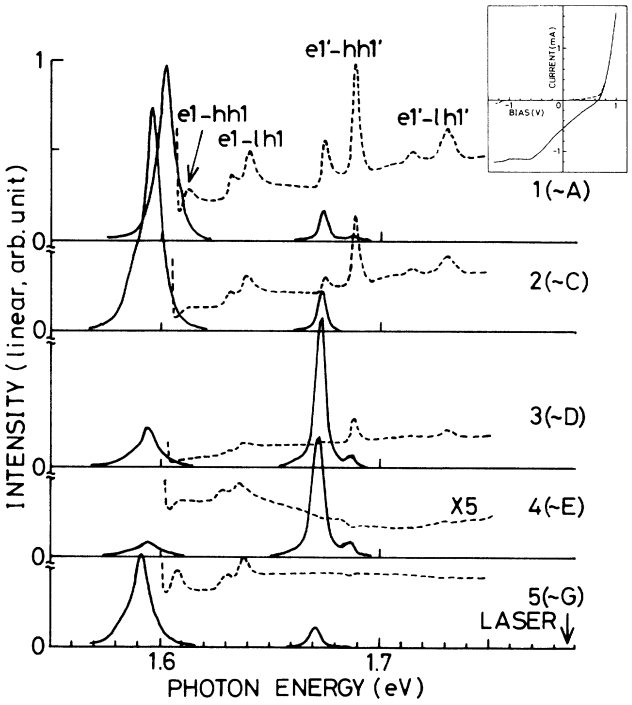


FIG. 3. Time-integrated photoluminescence (PL) and photoluminescence excitation (PLE) spectra of sample I measured at 20 K under several bias conditions: (1) flat band, (2) the beginning of the quasiresonance region, (3) the resonance, (4) the end of the quasiresonance region, and (5) the above-resonance condition, whose meanings are described in the text with representation by symbols $A$–G. The solid lines show the PL spectra of LQW and RQW and the arrow indicates the photon energy of laser used for the PL measurement. The dashed lines show the PLE spectra of LQW, where the detection photon energy is set to be 9 meV below the PL peak energy of LQW. The inset shows the gate current as a function of bias voltage, where the solid line indicates the photocurrent under illumination by laser with the same excitation condition (medium excitation) as that for the time-resolved PL measurement, and the dashed line indicates the dark current.

Solid lines in Fig. 3 show the PL spectra of LQW and RQW and the dashed lines show the PLE spectra of LQW. The arrow indicates the photon energy of the laser used for the PL measurement.

Each PL spectrum has two peaks whose intensities depend strongly on bias. These peaks are PL peaks from respective QW's. The PLE spectra of LQW show a series of exciton peaks in the PLE spectra of LQW; their assignment is indicated in the figure. It is noteworthy that the peaks associated with the excitonic absorption in RQW appears in spectra 1–3; this implies that some fraction of the electrons photogenerated in RQW are transferred to LQW and contribute to the luminescence. Note that each exciton peak is split into doublet structures, which is due to the well-width difference of one monolayer ($=2.83$ Å).[26] Since the PL from each QW comes mainly from the lower energy peak of the doublet, most of the photogenerated electrons relax to the region of the lower energy level and then radiatively recombine.

Now we present in Fig. 4(a) the measured decay times $\tau$ of the PL peaks from the two QW's of sample I as functions of applied voltage $V_a$. Similarly, the time-integrated intensities $I$ of the two PL peaks are shown in Fig. 4(b). Note that $\tau$ and $I$ vary sensitively with $V_a$, indicative of a strong variation of the tunneling process as the relative position of the two quantum levels is varied. The flat-band condition is reached at $V_a \sim +0.7$ V as indicated in the inset of Fig. 3 where the $I$-$V$ characteristic of the structure is plotted.

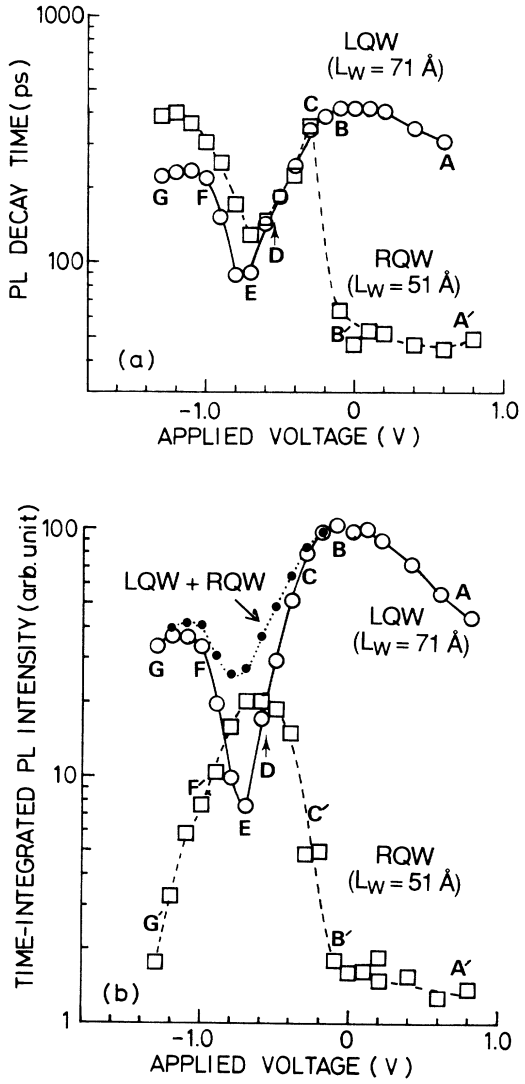


FIG. 4. (a) Photoluminescence decay time and (b) time-integrated photoluminescence intensity of sample I as functions of applied voltage at 20 K. Open circles (solid line) are for LQW and open squares (dashed line) for RQW. Solid circles (dotted line) are the sum of the PL intensities of LQW and RQW. The excitation wavelength is 6940 Å. The symbols $A$–$G$ indicate the typical conditions of tunneling, which are described in the text.

Before discussing these data in detail, we examine first how the external voltage $V_a$ affects the potential profile in this double-QW structure. If the concentration of photogenerated carriers is sufficiently low, then the voltage $V_a$ is supported evenly by the undoped part of the sample between the metal Schottky contact and the underlying $n^+$-type GaAs region. In such a case, the electric field $F_{QW}$ between the two QW's can be easily estimated, since the field is uniform and is equal to $(0.7\ \text{V}-V_a)/d_{und}$, where $d_{und}$ is the thickness of the undoped region. When the concentration of photogenerated carriers increases, then these carriers start to screen the external field and give rise to a field nonuniformity. In fact, it was found that the bias voltage dependence of PL intensity shown in Fig. 4(b) is somewhat dependent on the power intensity $P$ of the excitation laser. To clarify this situation we also measured the PL intensities as a function of $V_a$ by using a weaker excitation ($\sim 1$ W/cm$^2$) with a power intensity $\frac{1}{5}$ of that for Fig. 4(b). The data are shown by solid circles and solid squares in Fig. 5, where the data of Fig. 4(b) are also replotted with open circles and open squares for comparison. Note that the two sets of data are quite similar to each other except that the voltage scale is displaced about 0.5 V.

This implies that when the excitation power is medium ($\sim 5$ W/cm$^2$), the effective electric field $F_{QW}$ in the QW region remains nearly constant in the range of $V_a = 0.7-0.2$ V. Hence, the local field $F_{QW}$ is then approximately $(0.2\ \text{V}-V_a)/d_{und}$. In the present experiment, while we could perform the time-integrated measurement of PL intensities with the weaker excitation power, we had to perform the time-resolved PL measurement with the medium excitation power ($\sim 5$ W/cm$^2$) because of the limitation of signal-to-noise quality of the data. Hence, we always consider this voltage-offset effect.

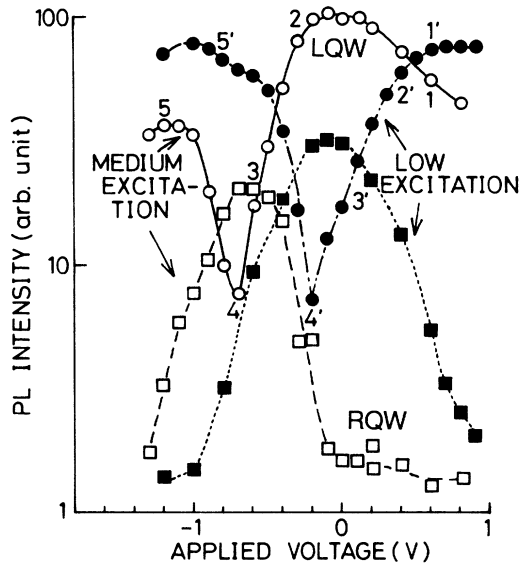


FIG. 5. Time-integrated photoluminescence (PL) intensities of sample I as functions of applied voltage for two different excitation powers. Open circles (solid line) represent PL intensity for LQW and open squares (dashed line) for RQW at the medium excitation power (5 W/cm$^2$) used for the time-resolved measurement. Solid circle (dash-dotted line) and solid squares (dotted line) represent PL intensities for LQW and for RQW, respectively, measured with a lower excitation power (1 W/cm$^2$). The numbers 1-5,1'-5' indicate the points where data in Fig. 3 were taken, corresponding to the various resonance conditions.

This voltage shift is caused by two factors, as will be described in detail later; the first is the Ohmic voltage drop $\Delta V = I_{ph} R_S$ which is caused by the series resistance $R_S$ ($\sim 140\ \Omega$) and the photocurrent $I_{ph}$ associated with the photoexcitation; the second and more important is due to hole accumulation in the QW region, which partly screens the external field. This hole accumulation results mainly from the leftover holes in LQW that fail to recombine with electrons that have leaked out by tunneling. These holes consist of those generated in the QW's and those injected from the undoped GaAs region. The holes will be accumulated over many periods of laser pulses and influence mostly the steady-state field distribution, since the hole transport from the QW's to the outside will occur in a much slower time scale than the radiative recombination and electron tunneling processes. Note that this hole accumulation does not directly influence the tunneling dynamics of the electrons since the height of the AlAs potential barriers is scarcely modulated; the change of the potential height caused by the hole accumulation is estimated to be less than 50 meV, which is much smaller than the potential barrier height ($\sim 1$ eV) of AlAs. The effect of the hole accumulation will be discussed more in Sec. III A 3 a. Note also that the radiative recombination process in our case occurs under the condition where the hole concentration is much higher than that of electrons. This situation is favorable since the recombination rate $1/\tau_{rec}$ is independent of hole concentration and the PL intensity is proportional to the electron density at low temperature (20 K), where the carriers are under the degenerate condition.[27,28]

As explained in our earlier work,[15,16,24] it is convenient to discuss the data of Fig. 4 in several different regions. The region $A-B$ in Fig. 4 corresponds to one of the off-resonant conditions, which we refer to as "below resonance" since the ground level of LQW is well below that of RQW. In the region between $C$ and $E$, the two ground levels come close to each other (quasiresonance), while the exact resonant condition is believed to be established at $D$, as will be discussed later. The other off-resonant condition, which we refer to as "above resonance," is reached in the region $F-G$, where the ground level of LQW is way above that of RQW. In the following, we discuss in detail the electron dynamics in each region, and compare the experimental data with theoretical models.

### A. Tunneling dynamics under quasiresonance condition ($C-E$)

In the region between $C$ and $E$, the measured carrier lifetimes $\tau_L$ and $\tau_R$, and PL intensities $I_L$ and $I_R$, vary

sensitively with $V_a$. Note in this region that the lifetime $\tau_L$ of LQW is almost the same as that $\tau_R$ of RQW, suggesting that the communication between the two QW's is frequent. The lifetimes $\tau_L$ and $\tau_R$ decrease rapidly as $V_a$ is reduced. At the end of this region ($E$), $\tau_L$ decreases down to 90 ps. The observed variation of lifetime indicates that the tunneling process dominates the lifetime, and that the tunneling rate varies strongly with $V_a$ since the radiative recombination lifetime $\tau_{\rm rec}$ should not vary too much with $V_a$ in these narrow QW's and is around 400–500 ps. In fact, the measured $\tau_{\rm rec}$ is $\sim$400 ps (Ref. 27) under the flat-band condition, and $\tau_{\rm rec}$ is estimated to increase to $\sim$500 ps or longer for the above-resonance condition from the measurement of PL decay time in a double-QW structure with a thick ($=$100 Å) central barrier with an electric field.

Figure 4(b) indicates that the PL intensity $I_L$ of LQW decreases monotonically with decreasing $V_a$, while the PL intensity $I_R$ of RQW increases and reaches its maximum. At the end of this region ($E$), $I_L$ decreases to approximately $\frac{1}{3}$ of $I_R$. (Note that $I_L$ becomes almost equal to $I_R$ at $D$, where the exact resonance is reached, as will be described later.) We compare these data with theoretical predictions to clarify the tunneling mechanism in this region. We first examine the direct tunnel escape model (or coherent tunneling model); this idealized model is known to describe adequately the key features of resonant tunneling current in double-barrier diodes,[29,30] where the energy distribution of incident electrons is usually far greater than the effective width of transmission resonance peak. We point out that electron transport in double-QW structures under quasiresonant conditions cannot be explained by this model, but can be accounted for successfully by the relaxation-dominant model to be described later.

### *1. Direct tunnel escape model (coherent tunneling model)*

As shown in inset (a) of Fig. 6, the wave function originating from the ground level $E_{L1}$ of LQW is mainly confined in LQW. Some part of this wave function, however, penetrates into RQW and leaks out to the region of the right electrode. Hence, this state can be viewed as a quasibound state. The wave function of this state changes with applied field as follows. When the ground level $E_{L1}$ of LQW is brought close to but slightly below that $E_{R1}$ of RQW, the wave function starts to penetrate appreciably into RQW, which should result in an appreciable increase in the escape rate by direct tunneling. Under the exact resonant condition, the wave function is almost equally distributed in both QW's [inset (b)], and hence the tunnel escape rate from LQW to the outside should reach its maximum. When the ground level of LQW is slightly above that of RQW, the penetration of the wave function into RQW should diminish again [inset (c)], and the direct tunnel escape rate should decrease. We examine in the following this direct tunnel escape model (coherent tunneling model) by calculating the tunnel escape time on the basis of this model and compare it with the experimental data.

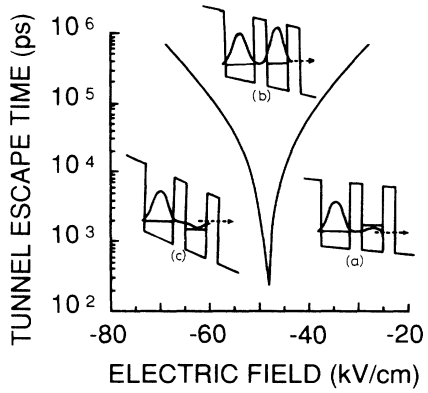


FIG. 6. The tunneling time of electrons in sample I from the left well (LQW) through the right well calculated for the direct tunneling escape process as a function of bias electric field. The inset illustrates the direct (coherent) tunneling escape processes of electrons from the left well (LQW) through the right well (RQW): (a) at slightly below resonance, (b) on resonance, and (c) at slightly above resonance.

The tunneling escape time from the left well to the outside (through RQW) was calculated in the following way on the basis of the two-band tight-binding approach. This approach includes nonparabolicity effects in the conduction band and varying electrostatic potential across the structure.[31] For a given voltage or electric field $F_z$, we assume that a free electron wave with a normalized amplitude is incoming from the "outside" region on the right side of RQW into the double-QW structure. Then, the wave function $\Psi(z)$ in the entire region was calculated as a function of incoming electron energy $E_z$. The square $|\Psi|^2$ of this wave function was integrated spatially over the regions of LQW and RQW separately to obtain the probability densities $\rho_L$ and $\rho_R$ in LQW and RQW as functions of incoming energy $E_z$. These curves, $\rho_L(E_z)$ and $\rho_R(E_z)$, have peaks at the energies of the resonances in LQW and RQW. The line shapes are characteristic Lorentzian line shapes typical of resonant tunneling transmission curves. The energy widths $\Gamma_L$ and $\Gamma_R$ of these resonance curves or the FWHM of the peaks represent the lifetime $\tau$ of these quasibound states; hence the escape time of electrons from LQW to outside by the direct tunneling process can be determined as $\hbar/\Gamma_L$.

Note that in a strict sense, the present calculation deals with the escape time of the quasibound state $\Psi$ (energy eigenstate in the total system) associated mostly with the ground level of LQW in the double-QW structure, and not that of the localized state $\Phi_L$ (eigenstate of a single QW) in LQW. In the case where electrons are initially created in the localized state of LQW, those electrons experience the tunneling oscillation process between the localized states of each QW (Appendix B). However, the results of the present calculation remain valid even for that case. This is because the tunnel escape process to the outside is not directly influenced by the oscillatory nature of the electron density, but is primarily deter-

mined by the time average of the electron density for the present case in which the oscillation period is much shorter than the direct tunnel escape time to the outside, as described in detail in Appendix C.

Now we present in Fig. 6 one example of such a calculation for sample I, where the direct tunneling time $\tau_L^{\rm dir}$ is plotted as a function of electric field $F_z$. As expected, the tunnel escape time $\tau_L^{\rm dir}$ becomes minimum ($\sim$230* ps) at resonance, and the width $\Delta F_z$ of the resonance peak is comparable to the energy splitting (0.57 meV, estimated by the two-band tight-binding approach) of the two coupled levels at the resonance divided by the average separation (92 Å) of the two QW's. The calculated escape time $\tau_L^{\rm dir}$ of the coupled QW's at resonance ($\sim$230* ps) is nearly two times as large as the calculated escape time $\tau_B$ ($\sim$110* ps) of electrons in a single 51 Å QW to the outside through a barrier of 31.1 Å. (Note that quantities accompanied with a superscript asterisk change somewhat if a barrier thickness is different from the designed value, as will be discussed later.) This relation, $\tau_L^{\rm dir}/\tau_B \approx 2$ at resonance is quite understandable since the flux of electrons hitting the rightmost barrier is reduced by a factor of 2 for the coupled QW structure at resonance as compared with that of a single QW. This is because the fraction of the electron wave function is split equally over the two QW's and the fraction in RQW is about one-half of the total at resonance. It is worth noting that even in the case that electrons are distributed in both of symmetric and antisymmetric states at 20 K, the net tunneling time also becomes twice $\tau_B$ since the tunneling times of the respective states equally become twice $\tau_B$. Note also that in a more general case, including the off-resonant condition, the direct tunneling escape time of electrons in a particular quantum state $\Psi_L$ of coupled QW's should be approximately equal to $\tau_B/P_R(\Psi_L)$, where $P_R(\Psi_L)$ is the fraction of the wave function $\Psi_L$ residing in the right QW.

If the time constant $\tau_L^{\rm dir}$ of the tunneling escape process is 230* ps as the model predicts, then this tunneling process should make a greater contribution than the radiative recombination process, which has a typical time constant $\tau_{\rm rec}$ of 400 ps at low temperatures. In this case, the PL intensity $I_L$ of LQW should decrease at resonance by a factor of $\sim$0.4 as compared to the off-resonant case, since the relative probability of the radiative recombination is given by $(1/\tau_{\rm rec})/(1/\tau_{\rm rec}+1/\tau_L^{\rm dir}) \sim (1/400\ {\rm ps})/(1/400\ {\rm ps}+1/230^*\ {\rm ps})$. Note here that the time-integrated PL intensity should be nearly proportional to the ratio of the radiative recombination decay rate $1/\tau_{\rm rec}$ over the total decay rate $1/\tau_{\rm rec}+1/\tau_L^{\rm dir}$ including the tunneling rate.

A similar analysis is applicable to the photoluminescence associated with the ground level $E_{R1}$ of RQW as long as the relevant roles of the two wells are properly exchanged. Once the fraction $P_R(\Psi_R)$ of electron wave $\Psi_R$ residing in RQW is known, then the tunneling escape time $\tau_R^{\rm dir}$ is approximately given by $1/\tau_R^{\rm dir}=P_R(\Psi_R)/\tau_B$. Hence, the tunneling escape time of electrons associated with the ground level of RQW is predicted to approximately double [$\tau_B$ ($\sim$110* ps) to $\sim 2\tau_B$ ($\sim$230* ps)], when the level is brought to the resonance. As a consequence, the time-integrated PL intensity $I_R$ should increase approximately double ($\sim$1.7), and is expected to become equal to that $I_L$ of LQW when the level is brought to the resonance, where $P_R(\Psi_R)=P_R(\Psi_L)=0.5$ and $\tau_R^{\rm dir}=\tau_L^{\rm dir}=2\tau_B$. Hence, this model predicts that the PL intensities $I_L$ and $I_R$ of the two QW's should vary with the applied voltage as schematically shown by the solid and dashed lines of Fig. 7.

If the effective thickness of the right barrier is thinner than the planned value by 0.5 ML or 5% of the barrier thickness, then the relevant tunneling times (marked by the asterisk in the text) will be shortened to 70% of the original values. In such a case, $\tau_B$ should be about 80 ps and $\tau_L^{\rm dir}$ about 160 ps. For such a case, the changes of PL intensities associated with resonance will be somewhat greater than those just discussed: $I_L$ should be reduced by a factor of 0.3 (instead of 0.4), while $I_R$ should increase nearly by a factor of 2.

Here we also note that for a realistic interpretation of the measured data of Fig. 4 one must take into account the presence of a well-width fluctuation of 1 ML (=2.83 Å) as indicated by the PLE spectra of Fig. 3. For a sample of this kind the measured $V_a$ dependence of $I_{\rm PL}$ is the superposition of $I_{\rm PL}$-versus-$V_a$ curves coming from different areas of the QW's. This will be discussed later.

Now we compare the experimental results with the direct tunneling model by examining the dependences of tunnel escape time $\tau$ and PL intensity $I$ on applied voltage $V_a$. Although the $V$-shaped dependence of lifetime $\tau_L$ on $V_a$ is seen in both experiment and theory, we note that there are some important discrepancies. Here we assume that resonance is reached at point $E$ of Fig. 4 since the direct tunnel escape model predicts that the tunnel escape time of LQW should become minimum at resonance. The first noteworthy discrepancy is that the PL lifetimes of the two QW's are no longer equal at point $E$, while they should be the same at resonance. Furthermore, the minimal value of the measured lifetime is 90 ps

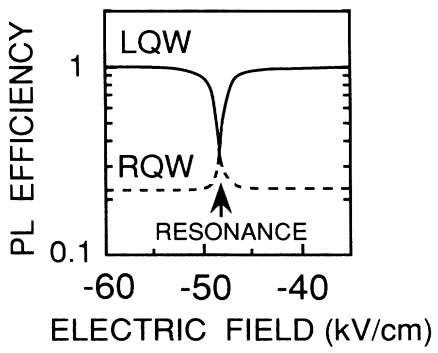


FIG. 7. Schematic illustration of the time-integrated PL intensity of each QW in sample I as a function of applied voltage, expected in the direct (coherent) tunneling escape process.

at point $E$ [Fig. 4(a)], shorter than the prediction (230 ps).

Discrepancies are found also in the observed dependences of the PL intensity on $V_a$, as explained below. As discussed earlier and summarized schematically in Fig. 7, the model predicts that the PL intensity of LQW should decrease at resonance by a factor of $\sim 0.4$ (or 0.3*) from the off-resonant value, and become equal to that of RQW, while the PL intensity of RQW is predicted to approximately double at resonance from the off-resonant value. These predictions do not agree with the experiment; the observed dependence of PL intensity on $V_a$ [Fig. 4(b)] was far stronger than the predictions, and the PL intensity of LQW at point $E$ is as small as $\frac{1}{3}$ of that of RQW in contrast to the prediction that they should be equal if we consider point $E$ as the resonant point. These discrepancies indicate that the actual electron tunneling is dominated not by the direct tunneling mechanism alone but is strongly influenced by another mechanism. Note especially that point $E$ should not be the exact resonant point, as will be discussed in the next section.

### 2. *Scattering-assisted tunnel escape process*

As discussed in Sec. III A 1 the direct tunnel escape model (or coherent tunneling model) is not adequate to explain the experimental results on the tunnel escape process in the double-QW structure. It is reasonable to consider effects of scattering since the scattering time is usually far less than the tunneling escape time ($> \sim 100$ ps) in our structure. Indeed, the importance of scattering in the interwell tunneling process was recently emphasized by the theoretical work of Ferreira and Bastard.[32] In the following, we investigate a model which takes into account the scattering and energy relaxation between the two quasibound QW states, and the subsequent tunneling to the outside.

First, we examine the time constant for the scattering-assisted transition between the two lowest quantum states, which are associated mainly with the ground levels of the two quantum wells. We discuss, in particular, how this transition time changes with electric fields. This transition time is generally determined by the slower of two relevant processes: the tunnel oscillation process with period $T_{\rm osc}$ (Appendix B) and the interlevel scattering process with time constant $\tau^{\rm scatt}$, because both must occur in series for the interwell transport to take place. In our sample, the interlevel scattering time $\tau^{\rm scatt}$ dominates the transition time since $\tau^{\rm scatt}$ is almost always much longer than the tunneling oscillation period $T_{\rm osc}$. An exceptional case appears only in a very small region near the exact resonance condition, where $\tau^{\rm scatt}$ (less than several picoseconds) may become comparable to the oscillation period ($\leq 7$ ps), as described below.

Suppose there exist two quantum levels or eigenstates $E_+$ and $E_-$ in a double-QW structure with wave functions $\Psi_+$ and $\Psi_-$; the transition rate between them by some scattering potential $V_{\rm scatt}$ should be proportional to $|\langle \Psi_+ | V_{\rm scatt} | \Psi_- \rangle|^2$. In the present case, the two wave functions $\Psi_+$ and $\Psi_-$ are expressed as linear combinations of the ground levels of the respective wells (See Appendix A), and the coefficients of the combinations change strongly with bias, whereas $V_{\rm scatt}$ can be assumed to be nearly constant ($V^0_{\rm scatt}$) in the bias range of the quasiresonance condition. Hence, the matrix element is roughly $V^0_{\rm scatt}$ multiplied by the overlap integral $\langle \Psi_+ | \Psi_- \rangle$ and, consequently, the electric field dependence of the scattering rate $1/\tau^{\rm scatt}$ is primarily determined by the overlap integral between the wave functions $\Psi_+$ and $\Psi_-$.

Note that the overlap integral over all space is zero due to orthogonality. The relevant quantity for estimating the scattering time $\tau^{\rm scatt}$ is the overlap integral over one well or one barrier. This is because the major scattering potentials in one well or one barrier should be mostly independent or incoherent with the others for such important scattering processes as electron-phonon scattering and interface roughness scattering.

By using the equations in Appendix A, the overlap integral in one well is written as $|\langle \Psi_+ | \Psi_- \rangle|^2$ (well) $= |a^L_+ a^L_-|^2 = |a^R_+ a^R_-|^2$ and the overlap $|\langle \Psi_+ | \Psi_- \rangle|^2$ (barrier) in the central barrier is written as $|(a^L_+ a^R_- + a^R_+ a^L_-)\langle \Phi_R | \Phi_L \rangle|^2$, where $\Phi_R$ and $\Phi_L$ are the unperturbed localized states in each well, and $a^j_i$ represents the mixing coefficients of the localized states in each eigenstate. In our sample, a numerical estimate indicates that the integral over one well is dominant compared to the overlap in the barrier. Hence, $1/\tau^{\rm scatt}$ should be roughly proportional to $|a^L_+ a^L_-|^2$ ($= 1 a^R_+ a^R_-|^2$). Note that the absolute scattering time is determined by the intrinsic scattering strength, which depends on the scattering mechanism. Qualitatively, this scattering process in our structures has some similarity to the intrasubband scattering in a single QW in the sense that the relevant initial and final wave functions for motion perpendicular to the epitaxial layers have nearly the same shape in both scattering events. Hence, at resonance ($a^j_i \sim 1/\sqrt{2}$), $\tau^{\rm scatt}$ is expected to be comparable to that of the intrasubband scattering time, which is estimated to be less than several picoseconds from the calculated and/or measured mobility value.[33]

The dependence of $\tau^{\rm scatt}$ on electric field is calculated and is shown in Fig. 8; here the minimum value of $\tau^{\rm scatt}$ is normalized to be 1 ps, which is a typical order of magnitude of the time constant of intrasubband scattering in QW's. As Fig. 8 shows, $\tau^{\rm scatt}$ is strongly dependent on electric field $F_z$; $\tau^{\rm scatt}$ increases significantly when $F_z$ deviates from the resonant point by some value $\Delta F_z$, which is equal to the energy splitting $\Delta E_{\rm spilt}$ of the two coupled states divided by the average separation (92 Å) of the two wells.

These considerations indicate that on the resonance and in its vicinity (the quasiresonance condition), the interwell electron-transport process occurs within several picoseconds in the present sample. Hence, under the quasiresonance condition, a quasiequilibrium distribution of electrons should be reached between LQW and RQW since the transition time is much faster than the time for tunneling to the outside of the wells. Consequently, the time evolution of the electron concentration in each well is dominated mainly by the electron tunneling to the outside while the electron concentrations $N_L, N_R$ in the left

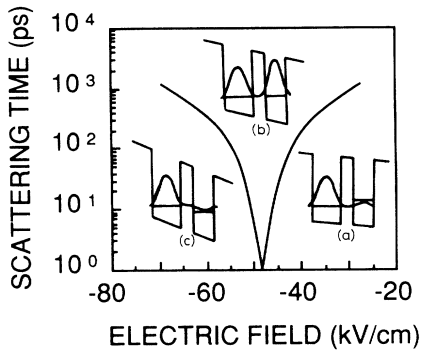


FIG. 8. The dependence of interlevel scattering time in sample I on bias electric fields calculated from the overlap integral between the electron wave functions of each QW. The minimal scattering time is set to be 1 ps. The inset illustrates this process under the conditions of (a) "slightly below" resonance, (b) on resonance, and (c) "slightly above" resonance.

and right well are in quasithermal equilibrium, and their ratio $r=N_L/N_R$ should be approximately equal to $\exp[-(E_{L1}-E_{R1})/k_BT]$. In the case that there are some well-width fluctuations, the ratio should be redefined by the ensemble average $\langle \exp(-E_{L1}/k_BT)\rangle_{av}/\langle \exp(-E_{R1}/k_BT)\rangle_{av}$, which is the average over various areas where the quasiresonance is established.

Under such a quasiequilibrium condition, the electrons tunnel to the outside with a time constant, which should be determined as follows:

$$\frac{d(N_L+N_R)}{dt}=-\frac{N_R}{\tau_B}=-\frac{(N_L+N_R)}{(1+r)\tau_B}\ , \tag{1}$$

where $\tau_B$ is the electron escape time by tunneling from the right well to outside through a single barrier. This $\tau_B$ can be calculated by the method described in Sec. III A 1 and is 110–80 ps for this case ($L_W=51$ Å, $L_B=31.1$–$29.7$ Å). Hence, the characteristic decay time is equal to $(1+r)\tau_B$, which becomes quite long when the greater fraction $r$ $(=N_L/N_R)$ of the electrons dwells in the left well. Similarly, PL intensities $I_R$ and $I_L$ from the right or the left QW's are given by $I_{L(R)}=N_{L(R)}/\tau_{rec}$, where $\tau_{rec}$ is the radiative recombination lifetime.

Using the above equations, the PL efficiencies of each QW, defined as the ratio $N_{PL}/N_{exc}$, can be predicted, where $N_{PL}$ is the density of the radiatively lost electrons in one well and $N_{exc}$ is the initial density of those electrons excited in the well by a laser pulse. The PL efficiencies are then predicted to be $\sim 2\tau_B/[\tau_{rec}+(1+r)\tau_B]$ for RQW and $\sim 2r\tau_B/[(\tau_{rec}+(1+r)\tau_B]$ for LQW, where $r$ is the ratio $N_L/N_R$ of the electron concentrations. Therefore, it is predicted that at resonance (point $D$) where $r=1$, the luminescence from both wells should have the same intensities ($I_L=I_R$). One also expects that $I_L$ decreases when the ratio $r$ decreases as the applied voltage becomes more negative, while $I_R$ increases first and reaches a more or less constant value. This mechanism explains why $I_L$ becomes far less than $I_R$ at the edge (point $E$) of the resonant region. Throughout the quasiresonance condition, the lifetime of RQW is expected to be the same as that of LQW due to the fast relaxation between the two wells. In addition, the PL lifetime is expected to be twice $\tau_B$ at resonance and to decrease down to $\sim\tau_B$ at the edge (point $E$) of the resonant region because $r$ becomes nearly zero. These predictions agree well with the data.

The above discussion clarifies that interwell transport processes under the quasiresonant condition is very fast and creates a quasithermal equilibrium distribution of electrons by relaxation processes. Hence, the tunneling from the left QW to the outside via the right well is dominated mostly by scattering-assisted sequential processes. In addition, the resonance condition is interpreted to be reached on average at point $D$ in Fig. 4, where both the PL intensities and the lifetimes of the two QW's are equal to each other.

### 3. *Energy width and strength of resonance*

In this section, we discuss both the energy width and the strength of the resonant coupling in actual experimental situations, and how the inhomogeneous broadening affects them. We can define the effective width of the resonance from the experimental data of Fig. 4(a) by taking it to be half of the voltage range in which the lifetimes of the two QW's are nearly equal to each other. The width $\Delta V_a$ of the bias voltage thus determined is 200 mV. In order to translate the voltage width to the energy splitting between the ground levels of the two QW's, one must consider how the electric field is distributed across the undoped region.

*a. Field distribution and hole accumulation.* The calculation described in Sec. III A 1 predicts that the resonance condition is reached when electric field ($F_{QW}$) between QW's is $-47$ kV/cm. If the electric field is uniform, the bias voltage at resonance should be $\sim 0.1$ V [$=F_{QW}\times(1200$ Å$)+0.7$ V]. In contrast, the measured voltage is $-0.5$ V, which differs from the predicted value by 0.6 V. As discussed earlier, the major component of this discrepancy comes from the hole accumulation effect, which offsets the flat-band voltage by about 0.5 V. In fact, as shown in Fig. 5, the time-integrated PL intensities measured with low excitation light become equal for the two QW's at point 3, which indicates that the resonance is reached at the bias voltage of $+0.1$ V.

Next we discuss quantitatively the two mechanisms that may screen the external voltage and reduce the field $F_{QW}$. First, the Ohmic voltage drop across the electrode region is estimated to be less than 0.17 V because, as shown in the inset of Fig. 3, the series resistance $R_s$ is 140 Ω and the photocurrent is less than 1.2 mA. Hence this component is relatively small.

Next, we estimate quantitatively the effect of hole accumulation in the QW's. Some of the holes photogenerated in the QW's cannot recombine radiatively since some photogenerated electrons are lost by tunneling before recombining with the holes. In addition, some holes

photogenerated in the undoped GaAs layer are injected into the QW's because of the electric fields. Those leftover holes are accumulated mainly in LQW since the ground level of hole in LQW is lower than that of RQW. After the accumulation, holes are lost slowly through nonradiative decay processes such as tunneling, thermionic emission, and trapping into nonradiative centers. The density of these accumulated holes is then given by the product of the incoming flux of holes ($cm^{-2}s^{-1}$) and the lifetime determined by nonradiative decay processes. If we take the incoming flux to be $(1-2)\times10^{10}$ $cm^{-2}$ in each period (24 ns) of the laser pulse, and the lifetime of leftover holes to be 1 $\mu$s, the density $N_h$ of accumulated holes is expected to be $(4.2-8.3)\times10^{11}$ $cm^{-2}$. These holes in LQW screen the field by inducing an electric field between QW's by $\Delta F=eN_h/\epsilon=29-58$ kV/cm. If the hole density does not depend much on the bias voltage, the net effect is quite simple and gives rise to a voltage offset of 0.3–0.6 V in the PL-intensity–versus–$V_a$ curve. Hence, this hole accumulation effect explains successfully why the measured $V_a$ dependence of PL intensity depends on the excitation laser power $P$ and is shifted by about 0.5 V when $P$ was reduced. Note at this point that the change $\Delta F$ in the electric field $F_{QW}$ between the QW's can be estimated by taking this shift into account and is almost equal to the bias voltage change $\Delta V_a$ divided by the thickness ($=1200$ Å) of the undoped region.

*b. Resonance width and its broadening mechanisms.* The fact that the lifetimes of the two QW's are equal over the voltage range $\Delta V_a$ of 200 mV indicates that the interwell transport is quite efficient over the energy-level width of about 15 meV for the two QW's. This is because the average separation of the two QW's is 92 Å and accounts for only 7.7% of the total thickness of the undoped region ($\sim1200$ Å). This energy width $\Delta E_{expt}$ is much larger than the calculated energy splitting $\Delta E_{split}$ (0.57 meV) due to the resonant coupling and also far greater than the lifetime broadening $\hbar/\tau_{sc}$ caused by the scattering which is expected to be $\sim1$ meV.[34] Therefore, the effective resonance width $\Delta E_{expt}$ is determined by other mechanisms, such as (1) the energy-level broadening associated with well-width fluctuation, (2) the nonuniformity of the applied electric field, and (3) the nonuniform screening of electric field induced by photoexcited carriers in the QW's.

We examine the first contribution;[12] the heterointerface quality of the QW structure can be estimated by the lineshape analysis of the PLE spectra of Fig. 3. There the PLE peaks for each exciton absorption are split into relatively sharp doublet structures, which is typical of QW's prepared by MBE with growth interruption.[35] The sharp splitting indicates that the top (AlAs on GaAs) interface of the QW's is flat over a wide area with a step interval of more than 1000 Å,[35] which is larger than the exciton diameter ($\sim200$ Å). When a well-width difference $\Delta L_W$ of 1 ML exists, the ground level energy of electron will differ by an amount $\Delta E_{ML}$. This difference $\Delta E_{ML}$ is 5 meV for LQW (when estimated from an energy splitting of 8.2 meV for an $e$1-lh1 exciton), and 10 meV for RQW (from the corresponding splitting energy of 14.4 meV for an $e$1-hh1 exciton). The widths of each PLE peak are mainly ascribed to the roughness of the bottom (GaAs on AlAs) interface of the QW's, where the lateral size of islands is less than 100 Å.[35,36] The observed broadening can be split into the level fluctuation of electrons and that of holes; the former $\Delta E_{rough}$ is estimated to be about 2.6 meV for both QW's when assessed from the measured FWHM ($\sim4.8$ meV) of the PLE peak of $e$1-lh1 in LQW and that ($\sim3.4$ meV) of $e$1-hh1 in RQW.

These splittings $\Delta E_{ML}$ and broadenings $\Delta E_{rough}$ of the electronic levels in the present double-QW structures will certainly broaden the resonance condition. We refer to the two pairs of the quantum levels by $(E_{L1},E'_{L1})$ and $(E_{R1},E'_{R1})$, in which $E'_{L1}$ and $E'_{R1}$ denote the (higher) ground levels coming from the thinner regions of respective QW's, while $E_{L1}$ and $E_{R1}$ denote those lower ground levels coming from the thicker regions of the QW's. As the bias voltage is applied negatively from the flat-band condition, $E'_{L1}$ resonates first with $E_{R1}$. As the bias becomes more negative, $E_{L1}$ resonates with $E_{R1}$, then $E'_{L1}$ resonates with $E'_{R1}$, and finally $E_{L1}$ resonates with $E'_{R1}$. Since each of these four resonance modes overlaps with adjacent modes due to the level broadening $\Delta E_{rough}$, the resonance width will be broadened considerably and will be close to the sum (15 meV) of the energy splitting (5 meV for LQW and 10 meV for RQW).

The broadening may also result from a local variation of Schottky barrier height ($<\sim0.1$ eV) but this contribution is estimated to be only a few to several meV to the broadening of the resonance width. The broadening caused by the nonuniform distribution of carriers in the QW's is estimated to be less than several meV, because the variation of local potential profile caused by the polarization of photogenerated electrons is estimated to be 6 meV even at an electron concentration of $5\times10^{10}/cm^2$ while the density of photogenerated electrons in the QW is far below $5\times10^{10}/cm^2$.

*c. Inhomogeneity and interwell tunneling process.* Next, we examine how the inhomogeneous broadening $\Delta E_{expt}$ affects the interwell tunneling process. Although doublet structures were observed in the PLE spectra (Fig. 3), we assume that the resonance condition is dominated by a broad but single peak structure since the PL-intensity–versus–bias curves [Fig. 4(b)] agree with this assumption. The reason why the doublet structures are blurred in the PL–intensity–versus–bias curves is that both the level broadening in LQW and that in RQW contribute jointly to the broadening of the resonance curve. Now we discuss the influence of the broadening to the interwell tunneling based on this assumption. There are two possible regimes that might be important, depending on the relative rate of the perpendicular transport (or interwell tunneling normal to the quantum-well planes) to that of lateral transport (parallel to the planes). The first regime is one in which the lateral lengths of the inhomogeneity or the well-width fluctuation are so small that the time needed for carriers to equilibrate between different regions is negligibly small compared to the interwell tunneling time near the resonance. In this case the effective or observable interwell tunneling time, $\tau_T$(eff), becomes longer than the intrinsic tunneling time $\tau_T$(intrinsic) by a factor of $\Delta E_{expt}/\Delta E_{split}$, where $\tau_T$(intrinsic) represents

the interwell tunneling time in the absence of inhomogeneous broadening. Generally, $\tau_T$(intrinsic) corresponds to the longer time constant of the two serial processes, scattering-assisted interwell tunneling time and oscillation tunneling time, depending on the sample structures. This increase of $\tau_T$ originates from the fact that only a fraction ($=\Delta E_{\text{split}}/\Delta E_{\text{expt}}$) of the electrons can actually tunnel resonantly from one well to the other at a given time, assuming that the redistribution process of the electrons over a lateral area does not delay the process. Note here that this increase of the tunneling time occurs only for the resonant interwell process but does not directly affect the tunneling escape process to the outside.

The other regime is one in which the characteristic time needed for electrons to move laterally into an area where the resonant condition is fulfilled is far larger than the intrinsic interwell tunneling time. In this case the effective interwell tunneling time is determined by the lateral transport time needed for electrons to travel from nonresonant to resonant regions.

Our case is expected to be the former regime for the following reason. As discussed earlier, the inhomogeneous broadening of the resonant peak is dominated in our sample mostly by the well-width fluctuation. The relevant lateral size of such a fluctuation is that of the heterointerface roughness and is typically 100–1000 Å.[35,36] The transfer time of electrons across the lateral distance of 100–1000 Å with an energy of $k_B T$ ($\sim 2$ meV) is of the order of 100 fs to 1 ps, which is faster than or comparable to the interwell tunneling time. Therefore, the effective interwell tunneling time should be given by $(\Delta E_{\text{res}}/\Delta E_{\text{split}})\tau_T(\text{intrinsic}) \cong 30\tau_T(\text{intrinsic})$ and is predicted to be less than 50 ps. This value is still far shorter than the measured lifetime $\tau_L$ of LQW on and near resonance and, therefore, allows quasiequilibrium to be reached, which agrees with our interpretation of scattering-assisted tunneling described in the previous section.

In order to examine how the effect of resonant coupling varies with the thickness of the central barrier, we have performed similar measurements on another double QW (Sample III) having a thicker central barrier ($=56.6$ Å). The interwell tunneling time just on resonance for this sample should be determined mainly by the tunneling oscillation process because on the exact resonance the intrinsic oscillation tunneling time $\tau^{\text{osc}}$ (Appendix B) is calculated to be $\sim 96$ ps, which is much larger than the scattering-assisted interlevel transition time. However, the measured lifetime of electrons in LQW was nearly independent of the bias voltage and did not show any significant sign of resonant coupling. Hence, the effective interwell resonant tunneling time in Sample III is estimated to be significantly longer (more than $\sim 1$ ns) than the radiative lifetime ($\sim 400$ ps). This fact demonstrates that the contribution of the resonant tunneling is strongly suppressed in this sample. This is probably because even a small inhomogeneous broadening $\Delta E_{\text{expt}}$ of the quantum levels is adequate to blur or mask the intrinsic resonant effect, since the effective interwell tunneling time $\tau_T$ is greatly enhanced by a factor of $\Delta E_{\text{expt}}/\Delta E_{\text{split}} (> 100)$ over its intrinsic value, where $\Delta E_{\text{split}}$ is less than 0.1 meV.

### B. Off-resonant tunneling

#### 1. *Below-resonance condition* ( *A* – *B*)

As shown in Fig. 1(a), the tunneling rate from the left QW to the outside is expected to be reduced as the flat-band condition is established, where the ground quantum level of LQW is far below that of RQW. Indeed, the experimental value of the electron lifetime or PL decay time, $\tau_L$, of LQW is quite long (310–400 ps) in the region between *A* and *B* of Fig. 4(a), and is close to the radiative recombination lifetime $\tau_{\text{rec}}$. This implies that the tunnel escape time $\tau_T$ is greater than 1.4 ns if we subtract the contribution of the recombination path by using the relation $\tau_T = 1/(1/\tau - 1/\tau_{\text{rec}})$ with $\tau_{\text{rec}} \sim 400$ ps. The fact that the tunneling escape time of LQW is greater than 1.4 ns in this region shows that neither the direct tunneling nor the scattering-assisted tunneling process is very effective in this case, since the penetration of the wave function $\Psi_L$ to the outside through the two barriers and RQW is small.

The lifetime $\tau_R$ and the PL intensity $I_R$ of RQW in this region are very different from those of LQW, since the former two are strongly affected by two escape processes; one is the escape through the right barrier to the outside and the other process is the tunneling transfer process to LQW through the central barrier. The tunneling escape time $\tau_B$ to the outside is predicted to be 110–80 ps, as mentioned earlier. The tunneling transfer into LQW is difficult to estimate theoretically, since this is dependent both on the scattering and on the overlap of the relevant wave functions, as discussed earlier in connection with the scattering-assisted tunneling time $\tau^{\text{scatt}}$. This issue will be discussed in detail later in Secs. III B 2 *b* and III B 2 *c*. Here, we simply estimate this contribution of the process to the PL decay by using the following relation: $1/\tau_R = 1/\tau_B + 1/\tau_{\text{rec}} + 1/\tau_{\text{IW}}$, where $\tau_R$ is the measured PL decay time ($\sim 50$ ps or less) of RQW, $\tau_B$ is the simple tunneling escape time through a single barrier to the outside (110–80 ps), and $\tau_{\text{rec}}$ is the recombination lifetime ($\sim 400$ ps). The interwell tunneling time $\tau_{\text{IW}}$ thus determined is 120–200 ps and is somewhat longer than and yet comparable with the simple escape time $\tau_B$ to the outside. This is reasonable since the observed excitation spectrum of LQW has exhibited a structure that is associated with the exciton absorption of RQW. Under this off-resonant condition the PL efficiency of RQW should be given by $(1/\tau_{\text{rec}})/(1/\tau_R)$, which is less than $\frac{50}{400}$ or 13%. The observed PL efficiency of RQW shown in Fig. 4(b) is several percent and is in semiquantitative agreement, though there is some discrepancy.

Note that the tunneling transfer process from RQW into LQW for the below-resonance condition (case I) has some similarity to the opposite transfer process from LQW to RQW for the above-resonance condition (case II). While the first process from RQW to LQW has a time constant of 120–200 ps (case I), the other process from LQW to RQW has a somewhat longer $\tau$ of more than several hundred picoseconds for case II, as will be discussed in Sec. III B 2. The origin of the difference between these two cases is possibly in the penetration prob-

ability of the wave functions into the other well, in the contribution of the interface roughness scattering, and so on.

### 2. *Above-resonance condition (F–G)*

When the applied voltage $V_a$ gets more negative beyond the resonance voltage and raises the ground level of LQW above that of RQW, the tunneling rate from RQW to LQW becomes negligible and that from LQW to RQW is also reduced because of the breakdown of the resonance. This mechanism is responsible for the observed increase of both lifetime and PL intensity of LQW in the region between $E$ and $F$ of Fig. 4. In contrast, the PL intensity of RQW decreases, because the density of electrons in RQW decreases as the incoming electron flux from LQW decreases, and also the outgoing flux or rate from RQW to outside through the right barrier increases due to the field-induced lowering of the rightmost barrier. Surprisingly, the PL decay time $\tau_R$ of RQW increases in this region; this is due to the small incoming electron flux from LQW, which decays slowly with the lifetime $\tau_L$ of the electrons in LQW.

*a. Direct tunnel escape process.* The measured lifetime $\tau_L$ of LQW in sample I increases up to $\sim$240 ps for the above-resonance condition [Fig. 4(a)]. This indicates that the tunneling time $\tau_T$ is $\sim$460 ps, assuming a radiative recombination lifetime $\tau_{\rm rec}$ of $\sim$500 ps in this region of the electric field. Just as in the case of the resonance, the tunneling escape process for the above-resonance condition is expected to involve both direct (coherent) tunneling and scattering-assisted tunneling processes.

To evaluate each of the two contributions, we have performed for comparison a similar measurement of $\tau$ and $I$ on sample II, which has a thick (100 Å) right barrier. Note that the thick barrier suppresses or nearly prevents tunneling out of the double-QW structure. Consequently, the electron dynamics in sample II differs from that in the previous sample (sample I) mainly by the absence of the coherent (direct) tunneling escape process to the outside as long as recombination and other processes are the same for the two samples.

Figure 9 shows the measured intensity $I$ and decay time $\tau$ of photoluminescence from LQW in sample II. The lifetime for the above-resonance condition was $\sim$300 ps, whereas that of sample I was $\sim$240 ps [Fig. 4(a)]. By ascribing the difference of the decay rates ($\frac{1}{240}$ ps$-\frac{1}{300}$ ps) tentatively to the direct (coherent) tunneling process, the direct tunneling escape time $\tau_T^{\rm dir}$ from LQW to the outside through a 51 Å QW and thin (31 Å) barriers is estimated to be greater than $\sim$1.2 ns. Such a large value of $\tau_T^{\rm dir}$ indicates that the penetration of the wave function into RQW is quite small even under the above-resonance condition, where the field-induced lowering of the potential barriers starts to play a role. This implies that another tunneling mechanism may dominate the electron tunneling in sample I. We discuss electron scattering-assisted interwell tunneling of electrons in the next section.

*b. Scattering-assisted interwell tunneling process.* Scattering-assisted interwell tunneling processes exist

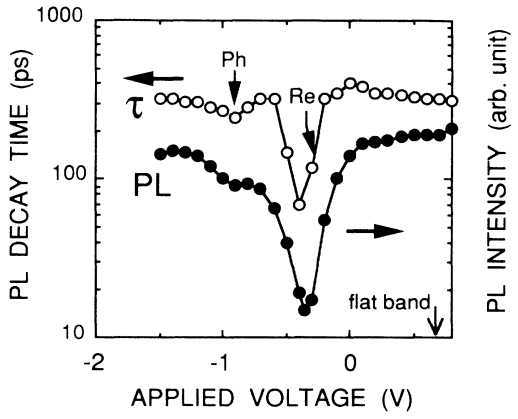


FIG. 9. PL decay time and time-integrated PL intensity of the left QW (LQW) as a function of bias voltage in a double QW (sample II) with a 31.1 Å central (interwell) barrier and a thick right (outside) barrier.

both in samples I and in II equally. Hence, we should be able to evaluate the scattering-assisted tunneling time $\tau_T^{\rm scatt}$ from the measured lifetime $\tau$ of sample II by using the relation $1/\tau = 1/\tau_T^{\rm scatt} + 1/\tau_{\rm rec}$. Since $\tau$ is $\sim$300 ps (Fig. 9) and $\tau_{\rm rec}$ is $\sim$500 ps, $\tau_T^{\rm scatt}$ under the above-resonance condition is estimated to be $\sim$800 ps. Note that $\tau_T^{\rm scatt}$ is much larger than the tunnel escape time ($\sim$100 ps) of electrons from the left QW to the unconfined three-dimensional states outside through the single thin (31 Å) barrier. This indicates that the electron tunneling from LQW to RQW for the above-resonance condition is not dominated by the transmission of a propagating wave through a single barrier but is strongly suppressed by the presence of the second (outside) barrier. The most important factor is the reduction of the overlap integral between the two wave functions associated with the ground levels of the respective QW's under the off-resonant condition, which has been discussed in Sec. III A 2 in connection with Fig. 8. This reduction of the overlap integral leads to a suppression of the scattering rate between the ground states of the two QW's and accounts for the reduction of the scattering-assisted tunneling rate $1/\tau_T^{\rm scatt}$.

Here we note two points that need future investigation. One should examine the reason why the estimated scattering-assisted tunnel time $\tau_T^{\rm scatt}$ from RQW to LQW is substantially shorter (120$\sim$200 ps, Sec. III B 1) than that ($\sim$800 ps) from LQW to RQW under the above-resonance condition. It might be related to the complicated band structure in the central AlAs barrier or to the difference of dominant scattering mechanisms in the two cases. The second point to be examined is the reason that the characteristic time $\tau_T^{\rm dir}$ for direct tunneling is relatively short ($\sim$1.2 ns) compared with the prediction for the above-resonance condition. Detailed analysis is needed to account for these two points.

*c. LO-phonon-assisted interwell tunneling process.* As shown by point Ph in Fig. 9, one notices that a dip struc-

ture appears in the measured lifetime and intensity of the PL from LQW of sample II when $V_a$ is near $-0.9$ V. The lifetime is $\sim 250$ ps at the minimum of the dip. This implies that the tunneling time is 500–1000 ps if we assume that other mechanisms such as radiative recombination contribute in parallel to the PL decay process with a time constant of 500–330 ps, which is the typical lifetime value for the off-resonance condition. Note that the difference of the bias voltage between the dip point Ph and the resonance point Re is 600 mV. This value corresponds to an electrostatic potential difference of 44 meV between the two QW's if we assume that uniform electric fields are supported across the undoped region of the sample. This is too large to be ascribed to well-width fluctuations. As will be described in the following, this dip is most likely to originate from a resonant enhancement of the scattering-assisted tunneling when the level spacing becomes close to the characteristic energy of the longitudinal-optical (LO) phonons.

Various scattering processes such as those by LO phonons, LA phonons, impurities, interface roughnesses, and electron-electron interaction may all contribute to the interwell transfer.[32,37,38] Among them, the scattering by LO phonons can be the most important when the energy-level spacing becomes close to the LO-phonon energy. The LO-phonon energy $\hbar\omega_{\mathrm{LO}}$ is 36 meV for bulk GaAs and 50 meV for bulk AlAs. The confinement of optical phonons in quantum wells and tunnel barriers may give rise to a series of new modes[39–42] including the interface phonon modes. Although they all have energies different from their bulk values, their energies $\hbar\omega_{\mathrm{LO}}$ all lie in the energy range from 30 to 50 meV. Hence, the tunneling rate from LQW to RQW is expected to increase when the energy of LQW becomes higher than that of RQW by $\hbar\omega_{\mathrm{LO}}$.

To examine the validity of attributing the observed dip to the LO-phonon-assisted tunneling, we discuss first the energy spacing $\Delta E_{LR}(=E_{L1}-E_{R1})$ between the two ground levels of the QW's at the bias point Ph, which was briefly discussed earlier. We tentatively assume here that the resonance is reached at point Re, where the PL intensities of the two QW's are equal, and suppose that the field is uniformly supported. Then, since the voltage difference $\Delta V_a$ between points Ph and Re is 600 mV, the electrostatic voltage drop between the centers of the two wells is estimated to be 44 meV or 7.3% of the total. For the energy spacing $\Delta E_{LR}$ of the ground levels, $\Delta E_{LR}$ is then calculated to be 44 meV$-\alpha$, where $\alpha$ is a correction term resulting from the difference in the Stark shifts of the two QW's and also from the change in the field screening caused by the accumulated holes mentioned earlier. This correction term $\alpha$ may be several meV. Hence, the energy spacing $\Delta E_{LR}$ (=44 meV$-\alpha$) is reasonably close to the confined LO-phonon energy (36 meV) of relatively thick GaAs quantum wells.

Next, we discuss which LO-phonon modes contribute predominantly to the tunneling. There are three possibilities: LO phonons confined in the GaAs well, those localized along the GaAs/AlAs interface, and those in the AlAs barrier. In order to estimate the relative magnitudes of the scattering rates due to these phonon modes, we calculate the overlap integral between the two relevant wave functions of the ground levels of each QW; we first calculate the overlap integral $I_W$ in the GaAs wells and that $I_B$ in the central AlAs barrier at a bias condition where $\Delta E_{LR}$ is $\hbar\omega_{\mathrm{LO}}$, following a method similar to that used in Sec. III A 2. The absolute squares of $I_W$ and $I_B$, denoted as $S_W$ and $S_B$ are, respectively, given by $|a_+^L a_-^L|^2+|a_+^R a_-^R|^2$ and $|(a_+^L a_+^R + a_-^R a_-^L)\langle\Phi_R|\Phi_L\rangle|^2$. Note that, for $S_W$, the contributions from both wells are added since the phonons in each well contribute independently.

The calculated $S_W$ is $1.3\times10^{-4}$ for $\Delta E_{LR}=36$ meV and $6.5\times10^{-5}$ for $\Delta E_{LR}=50$ meV. In contract, $S_B$ is found to be $1.3\times10^{-6}$ both at $\Delta E_{LR}=36$ meV and 50 meV. Note that $S_W$ is much larger than $S_B$ by a factor of 50 or 100. This indicates that LO phonons in the AlAs barrier contribute much less than those in the GaAs well to the phonon-assisted tunneling process at point Ph. Hence, one can conclude that the dominant role is played either by the confined GaAs phonons or interface phonons.

Concerning this interpretation, it is worth noting the bias dependence of the PL decay time when the bias is more negative than that of point Ph in Fig. 9. The tunneling rate is reduced as the bias voltage becomes further negative. This feature is not consistent with phonon scattering in the AlAs barrier, because the overlap integral $I_B$ in the barrier is nearly independent of bias (or $\Delta E_{LR}$). On the contrary, this feature is more consistent with the phonon scattering mainly in the quantum wells since the overlap integral $I_W$ in the well is inversely proportional to $\Delta E_{LR}$ and, therefore, should result in a reduction of the scattering-assisted tunneling rate as the bias is made further negative beyond point Ph. Since the interface phonon may have a sizable amplitude in the well region, the bias voltage dependence of the scattering rate should be semiquantitatively similar to that of the confined phonons in the GaAs. To unambiguously clarify the relative contribution of these two phonon modes, further study appears to be necessary.

Finally, we estimate from the experiment the characteristic time $\tau_{\mathrm{ph0}}$ of phonon scattering for the case when two electronic states have an overlap integral of unity. Then $\tau_{\mathrm{ph0}}$ is deduced as the product of the measured tunneling time $\tau_{\mathrm{phonon}}$ (500–1000 ps) and the square of the overlap integral $S_W$ ($\sim 1.3\times10^{-4}$) and is found to be 70–130 fs. This value is close to the phonon scattering time of those electrons in GaAs bulk or QW's with energy greater than optical phonon energy. Note that $\tau_{\mathrm{ph0}}$ for this sample is calculated to be $\sim 50$ fs with an assumption that the LO phonon is bulklike, following the work of Price.[43]

## IV. SUMMARY

The tunneling dynamics of electrons between a wide and a narrow QW and that from the wide well to the outside through the narrow QW were investigated by time-resolved PL spectroscopy. The measured lifetimes and PL intensities showed marked variations as the energy spacing or the coupling of two relevant quantum levels

was adjusted by electric fields between resonant and off-resonant conditions.

It is found that the rates of both interwell tunneling and tunneling escape from the wide QW to the outside are enhanced when the two levels were near resonance. The tunneling escape process near resonance is interpreted to be dominated by a scattering-assisted process, in which the fast ($<\sim 50$ ps) scattering-assisted interwell tunneling processes create a quasiequilibrium distribution of electrons between the two QW's while those electrons escape by tunneling rather slowly ($\geq 90$ ps) to the outside electrode. Consequently, the tunneling escape time is found to be minimized when the ground level of the wide QW is placed slightly above resonance, where the escape time becomes about half of that at resonance.

The intrinsic width of the resonance peak is typically 1 meV or less and far smaller than the inhomogeneous broadening of the ground levels in narrow QW's. Hence the effective width of the resonance peak is dominated by inhomogeneous broadening. As a consequence the effective interwell tunneling time is found to become larger than the intrinsic tunneling time. For example, for the case $L_B=57$ Å, the enhancement is estimated to be more than a factor of 10.

Under off-resonant conditions, the tunneling escape process from the wide well to the outside is reduced and its characteristic time is found to increase to more than $\sim 800$ ps. In addition, the interwell tunneling process assisted by the LO-phonon emission process is observed and its time constant is estimated to be 500–1000 ps for the present case, where the square of the overlap integral between the wave functions of the two QW's is of the order of $10^{-4}$. The LO phonons responsible for this process are suggested to be those phonons in the GaAs well region.

The study has also demonstrated that the interwell tunneling rate increases drastically at resonance and becomes far greater than the escape rate from a QW to unconfined 3D states in the bulk. In contrast, the interwell tunneling rate is suppressed substantially under the off-resonant condition and becomes far smaller than the escape rate from the QW to the outside. These features in the dynamics of the interwell tunneling result mainly from the interference of multiple reflected waves, and differ significantly from those in double-barrier resonant tunneling (RT) structures, where the tunneling escape process can be described well by the tunneling of oscillatory (confined) waves to unconfined states through a single barrier. This implies that if confined 2D states of electrons are formed in the accumulation layer of the emitter electrode of a double-barrier resonant tunneling diode, then the carrier buildup process may be affected by this energy-sensitive interwell tunneling process.

## ACKNOWLEDGMENTS

We wish to thank Dr. H. Akera and Professor T. Ando for useful discussions. We also thank T. Noda for collaboration and Professor Y. Arakawa and Professor K. Hirakawa for their support. This work is supported by a Grant-in-Aid from the Ministry of Education, Science, and Culture, and partly by the ERATO Grant for Quantum Wave Project from Research and Development Corporation of Japan.

## APPENDIX A: WAVE FUNCTIONS IN DOUBLE-QUANTUM-WELL STRUCTURES

In a coupled QW structure, the ground states $\Phi_L,\Phi_R$ of the two wells may couple and form two eigenstates $\Psi_+,\Psi_-$.[44] When the energies of $\Phi_L$ and $\Phi_R$ are apart, the eigenstates $\Psi_+,\Psi_-$ will be mostly localized in each well. At resonance, $\Psi_+$ and $\Psi_-$ will be the familiar symmetric and antisymmetric combinations. In general cases, $\Psi_+$ and $\Psi_-$ can be approximately expressed as linear combinations of unperturbed ground states $\Phi_L$ and $\Phi_R$:

$$\Psi_\pm = a_\pm^L \Phi_L + a_\pm^R \Phi_R \ , \tag{A1}$$

where the coefficients $a_\pm^L$ and $a_\pm^R$ depend on the bias field $F$. The Schrödinger equation can be written as the eigenvalue problem

$$\begin{bmatrix} E_L - E_\pm & -u \\ -u & E_R - E_\pm \end{bmatrix} \begin{bmatrix} a_\pm^L \\ a_\pm^R \end{bmatrix} = 0 \ , \tag{A2}$$

where $E_L = E_L^0 - eFd$, $E_R = E_R^0 + eFd$, $u$ is the coupling energy, and $2d$ is the distance between the center positions of each well. $E_L^0$ represents the unperturbed confinement energy of the ground state of LQW with no electric field, $E_R^0$ is that of RQW. The coupling energy $u$ is chosen to be 0.285 meV for sample I ($L_B=31.1$ Å) to give the correct energy splitting at resonance, which is separately calculated by the two-band tight-binding theory.

## APPENDIX B: TUNNELING OSCILLATION OF ELECTRON WAVE FUNCTIONS

As described in Appendix A, two eigenstates of a coupled-QW structure originate mainly from the ground states of the two wells and can be expressed as a linear combination of the two. In contrast to the stationary situation, one can dynamically use a short laser pulse to excite a valence electron in one well to a conduction-band state localized in the same well, even near the resonance condition. This can be done only if the energy width of the laser pulse or the coherence linewidth of the light (inverse of the coherence time) is set far greater than the energy splitting between the eigenstate energies. The laser pulse would then excite the electron into both eigenstates with the same amplitude and thus create a localized electron in one well. This electron would then tunnel into the other well at some rate. After a certain period, the electron would start to tunnel back into the original well, if the phase coherence time of the electron wave is much larger than the oscillation period. As a consequence, the electron density in one well will oscillate with time,[45] similarly to the behavior of optical waves in a coupled waveguide system. We analyze here this oscillation in a coupled-QW structure sandwiched by thick barriers on both ends as shown in the inset of Fig. 10; this system is

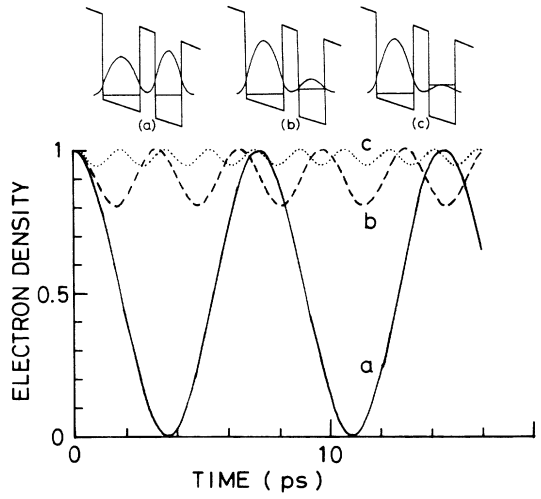


FIG. 10. The time variation of the electron density in LQW in the present coupled-QW structure [sample I or II: $L_W$(LQW)=71 Å, $L_W$(RQW)=51 Å, $L_B$(central barrier)=31 Å] at various bias electric fields: (a) on resonance, (b) slightly apart ($\Delta E_{LR}=1.14$ meV), and (c) further from the resonance ($\Delta E_{LR}=2.28$ meV).

easier to analyze but the essence of the interwell tunneling process in this system is the same as that in sample I, where the rightmost barrier is thinner.

The localized state in LQW prepared by a laser pulse can be written as a linear combination of the energy eigenstates as

$$\Psi_W(t=0)=\Phi_L=c_+\Psi_+ + c_-\Psi_-(|c_+|^2+|c_-|^2=1) . \tag{B1}$$

Hence, the time development of the electron state is written as[44]

$$\Psi_W(t)=c_+\Psi_+\exp\left[-i\hbar^{-1}E_+t\right] + c_-\Psi_-\exp\left[-i\hbar^{-1}E_-t\right] , \tag{B2}$$

where $E_+$ and $E_-$ are the energy of $\Psi_+$ and $\Psi_-$ states, respectively. As a consequence, the probability of finding electrons in the localized state of LQW is written as

$$P_L(t)=|\langle\Phi_L|\Psi_W(t)\rangle|^2 = 1-4|c_+|^2|c_-|^2\sin^2\left[\frac{E_--E_+}{2\hbar}t\right] , \tag{B3}$$

where all the constants $c_+$, $c_-$, $E_+$, and $E_-$ can be calculated using the analytic equations in Appendix A. Equation (B3) indicates that $P_L(t)$ oscillates with time in amplitude of $4|c_+|^2|c_-|^2$ and in period $T_{\rm osc}$ of $2\pi\hbar/\Delta E$, which is shown in Fig. 10. At resonance, the period and amplitude of the oscillation become maximal. As it deviates more from the resonance, both the period and amplitude decrease rapidly. Note that the period of the oscillation corresponds to the time needed to establish the eigenstate. Note also that the relevant time constant denoted as the oscillation tunneling time $\tau^{\rm osc}$ is the time in which the electron density reduces to half of the initial value, which is $\frac{1}{4}$ of $T_{\rm osc}$. Figure 11 shows the calculated oscillation period as a function of bias electric field.

## APPENDIX C: TUNNELING ESCAPE PROCESS ACCOMPANIED BY TUNNELING OSCILLATION

The calculation of the tunneling escape time in Sec. III A 1 deals with the escape time of the quasibound state $\Psi$ (energy eigenstate in the total system) associated with the ground level of LQW in the double-QW structure, and not that of the localized state $\Phi_L$ (energy eigenstate of a single QW) in LQW. However, electrons can be generated almost selectively in the localized state $\Phi_L$ in the left QW of the double-QW structure, when the excitation laser pulse is very short and its wavelength is appropriately chosen. In this case, electrons experience tunneling oscillation (as discussed in Appendix B) between the two localized states of both QW's during the tunneling escape process from the QW structure. Even for this case, where the localized state is initially created in LQW, our calculation of the tunneling escape time remains valid for the following reason.

In sample I, the maximum period of the oscillation that is realized at resonance is calculated to be 7 ps, as shown in Fig. 11. The period is much shorter than the direct tunnel escape time. This implies that the tunnel escape process is not directly influenced by the oscillatory nature of electron density but it is primarily determined by the time average of electron density. The average value of the fraction of the wave function in RQW can be estimated from the fraction $P_R(\Psi_L)$ of the wave function of quasibound state $\Psi_L$, where $\Psi_L$ represents one of the eigenstates $\Psi_+$ or $\Psi_-$ which belongs mainly to LQW. Consequently, the escape rate by the direct tunneling process should be well predicted by the theory based on the quasibound states, even when the localized state is excited.

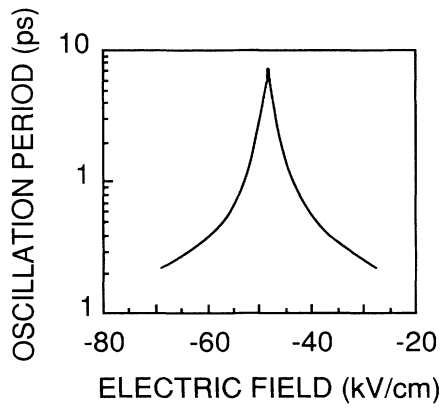


FIG. 11. The calculated period of the tunneling oscillation for samples I and II as a function of bias electric fields.

*Permanent address: Hughes Research Laboratories, Malibu, CA 90265.

[1]L. L. Chang, L. Esaki, and R. Tsu, Appl. Phys. Lett. **24**, 593 (1974).

[2]T. C. L. G. Sollner, W. D. Goodhue, P. E. Tannenwald, C. D. Parker, and D. D. Peck, Appl. Phys. Lett. **43**, 588 (1983).

[3]R. Tsu and L. Esaki, Appl. Phys. Lett. **19**, 246 (1971).

[4]For a review, see, for example, F. Capasso, K. Mohammed, and A. Y. Cho, IEEE J. Quantum Electron. **QE-22**, 1853 (1986).

[5]T. C. L. G. Sollner, P. E. Tannenwald, D. D. Peck, and W. D. Goodhue, Appl. Phys. Lett. **45**, 1319 (1984).

[6]M. Tsuchiya, T. Matsusue, and H. Sakaki, Phys. Rev. Lett. **59**, 2356 (1987).

[7]E. R. Brown, W. D. Goodhue, and T. C. L. G. Sollner, J. Appl. Phys. **64**, 1519 (1988).

[8]J. F. Whitaker, G. A. Mourou, T. C. L. G. Sollner, and W. D. Goodhue, Appl. Phys. Lett. **53**, 385 (1988).

[9]M. K. Jackson, M. B. Johnson, D. H. Chow, and T. C. McGill, Appl. Phys. Lett. **54**, 552 (1989).

[10]T. B. Norris, X. J. Song, W. J. Schaff, L. F. Eastman, G. Wicks, and G. A. Mourou, Appl. Phys. Lett. **54**, 60 (1989).

[11]S. Tarucha, K. Ploog, and K. v. Klitzing, Phys. Rev. B **36**, 4558 (1987).

[12]M. Tsuchiya, Ph. D. thesis, University of Tokyo, 1987.

[13]S. Tarucha and K. Ploog, Phys. Rev. B **38**, 4198 (1988).

[14]T. Tada, A. Yamaguchi, T. Ninomiya, H. Uchiki, T. Kobayashi, and T. Yao, J. Appl. Phys. **63**, 5491 (1988).

[15]M. Tsuchiya, T. Matsusue, and H. Sakaki, in *Ultrafast Phenomena VI,* Vol. 48 of *Springer Series in Chemical Physics,* edited by T. Yajima, K. Yoshihara, C. B. Harris, and S. Shionoya (Springer-Verlag, Berlin, 1988), p. 304.

[16]T. Matsusue, M. Tsuchiya, and H. Sakaki, *Quantum Wells for Optics and Optoelectronic (1989 Technical Digest Series Vol. 10)* (Opt. Soc. America, Washington, D.C., 1989), p. 266.

[17]G. Livescu, A. M. Fox, D. A. B. Miller, T. Sizer, and W. H. Knox, Phys. Rev. Lett. **63**, 438 (1989).

[18]D. Y. Oberli, J. Shah, T. C. Damen, C. W. Tu, T. Y. Chang, D. A. B. Miller, J. E. Henry, R. F. Kopf, N. Sauer, and A. E. DiGiovanni, Phys. Rev. B **40**, 3028 (1989).

[19]N. Sawaki, R. A. Höpfel, E. Gornik, and H. Kano, Appl. Phys. Lett. **55**, 1996 (1989).

[20]M. Nido, M. G. W. Alexander, W. W. Rühle, T. Schweizer, and K. Köhler, Appl. Phys. Lett. **56**, 355 (1990).

[21]B. Deveaud, F. Clerot, A. Chomette, A. Regreny, R. Ferreira, G. Bastard, and B. Sermage, Europhys. Lett. **11**, 367 (1990).

[22]T. Matsusue, M. Tsuchiya, J. Schulman, and H. Sakaki, *Extended Abstracts (in Japanese) of 50th Autumn Meeting of the Japan Society of Applied Physics, Fukuoka, 1989* (Japanese Society of Applied Physics, Tokyo, 1989), p. 1076.

[23]D. Y. Oberli, J. Shah, T. C. Damen, J. M. Kuo, J. E. Henry, J. Lary, and S. M. Goodnick, Appl. Phys. Lett. **56**, 1239 (1989).

[24]H. Sakaki, T. Matsusue, and M. Tsuchiya, IEEE J. Quantum Electron. **QE-25**, 2498 (1989).

[25]T. Matsusue, M. Tsuchiya, and H. Sakaki, presented in *1989 OSA Topical Meeting on Quantum Wells for Optics and Optoelectronics, Salt Lake City, 1989,* WD-1.

[26]H. Sakaki, M. Tanaka and J. Yoshino, Jpn. J. Appl. Phys. Pt. 2 **24**, L417 (1985).

[27]T. Matsusue and H. Sakaki, Appl. Phys. Lett. **50**, 1429 (1987).

[28]T. Matsusue and H. Sakaki, *Report of Seminar on Electrical Engineering at Institute of Industrial Science, University of Tokyo* (partly in Japanese) (Institute of Industrial Science, Univ. Tokyo, Tokyo, 1988), Vol. 38, No. 34, p. 6.

[29]M. Tsuchiya and H. Sakaki, Jpn. J. Appl. Phys. Pt. 2 **25**, L185 (1986).

[30]M. Tsuchiya and H. Sakaki, Appl. Phys. Lett. **49**, 88 (1986).

[31]J. N. Schulman and M. Waldner, J. Appl. Phys. **63**, 2859 (1988).

[32]R. Ferreira and G. Bastard, Phys. Rev. B **40**, 1074 (1989).

[33]K. Hirakawa and H. Sakaki, Phys. Rev. B **33**, 8291 (1986).

[34]L. Schultheis, A. Honold, J. Kuhl, K. Köhler, and C. W. Tu, Phys. Rev. B **34**, 9027 (1986).

[35]M. Tanaka and H. Sakaki, J. Cryst. Growth **81**, 153 (1987).

[36]H. Sakaki, T. Noda, K. Hirakawa, M. Tanaka, and T. Matsusue, Appl. Phys. Lett. **51**, 1934 (1987).

[37]B. Movaghar, J. Leo, and A. MacKinnon, Semicond. Sci. Technol. **3**, 397 (1988).

[38]H. W. Liu, R. Ferreira, G. Bastard, C. Delalande, J. F. Palmier, and B. Etienne, Appl. Phys. Lett. **54**, 2082 (1989).

[39]A. K. Sood, J. Menéndez, M. Cardona, and K. Ploog, Phys. Rev. Lett. **54**, 2115 (1985).

[40]A. K. Sood, J. Menéndez, M. Cardona, and K. Ploog, Phys. Rev. Lett. **54**, 2111 (1985).

[41]R. Fuchs and K. L. Kliewer, Phys. Rev. **140**, A2076 (1965).

[42]M. V. Klein, IEEE J. Quantum Electron. **QE-22**, 1760 (1986).

[43]P. J. Price, Ann. Phys. (New York) **133**, 217 (1981).

[44]See, for example, C. Weisbuch, in *Semiconductor and Semimetals,* edited by R. Dingle (Academic, San Diego, 1987), Vol. 24, Chap. 1.

[45]See, for example, E. O. Kane, in *Tunneling Phenomena in Solids,* edited by E. Burstein and S. Lundqvist (Plenum, New York, 1969), Chap. 1; S. Luryi, Solid State Commun. **65**, 787 (1988).